Medical Engineering and Physics 77 (2020) 60–68

Contents lists available at ScienceDirect

Medical Engineering and Physics

journal homepage: www.elsevier.com/locate/medengphy

Anthropomorphic and biomechanical mockup for abdominal aortic aneurysm

Zinan He[a,b], Rosaire Mongrain[a], Simon Lessard[b], Boris Chayer[b], Guy Cloutier[b,c], Gilles Soulez[b,c,*]

[a] McGill University, 845 Sherbrooke Street West, Montréal, Québec H3A 0G4, Canada
[b] Centre de recherche du Centre hospitalier de l'Université de Montréal (CRCHUM), 900 Rue Saint-Denis, Montréal, Québec H2X 0A9, Canada
[c] Université de Montréal, 2900 Boulevard Edouard-Montpetit, Montréal, Québec H3T 1J4, Canada

ARTICLE INFO

Article history:
Received 27 March 2019
Revised 8 September 2019
Accepted 15 December 2019

Keywords:
Abdominal aortic aneurysm
Endovascular repair
Hydrogel-based mockup
Biomechanics
Image processing

ABSTRACT

Abdominal aortic aneurysm (AAA) is an asymptomatic condition due to the dilation of abdominal aorta along with progressive wall degeneration, where rupture of AAA is life-threatening. Failures of AAA endovascular repair (EVAR) reflect our inadequate knowledge about the complex interaction between the aortic wall and medical devices. In this regard, we are presenting a hydrogel-based anthropomorphic mockup (AMM) to better understand the biomechanical constraints during EVAR. By adjusting the cryogenic treatments, we tailored the hydrogel to mimic the mechanical behavior of human AAA wall, thrombus and abdominal fat. A specific molding sequence and a pressurizing system were designed to reproduce the geometrical and diseased characteristics of AAA. A mechanically, anatomically and pathologically realistic AMM for AAA was developed for the first time, EVAR experiments were then performed with and without the surrounding fat. Substantial displacements of the aortic centerlines and vessel expansion were observed in the case without surrounding fat, revealing an essential framework created by the surrounding fat to account for the interactions with medical devices. In conclusion, the importance to consider surrounding tissue for the global deformation of AAA during EVAR was highlighted. Furthermore, potential use of this AMM for medical training was also suggested.

1. Introduction

Abdominal aortic aneurysm (AAA) is characterized by the dilation of the abdominal aorta due to a progressive wall degeneration and stiffening that are often associated with the development of intraluminal thrombus (ILT). It is an asymptomatic pathological condition that may lead to aneurysm rupture which carries an in-hospital mortality rate of more than 50% [1]. Rupture prevention is based on aneurysm exclusion which can be done either by open repair or by the less invasive endovascular repair (EVAR) using stent-grafts (SG). Both treatments present immediate as well as long-term risks to the patient and should be reserved to the cases where the risk of rupture outweighs surgical risks [2]. EVAR is often preferred because of its lower morbidity and mortality as compared with open repair (1.6% versus 5%) [3–5]. This advantage is lost after four years owing to excess late deaths in the EVAR group due to aneurysm complications, in particular endoleaks [5] (residual flow around the SG). Over the past two decades, the EVAR technology has evolved substantially to enhance procedural success and long-term durability. This has expanded the patient population that can be treated by EVAR [6]. Currently, patients with more challenging anatomies (short and angulated aneurysm neck) are treated outside the instruction for use, leading to an increase of adverse event and mortality [7]. More complex EVAR procedures are now performed to extend the sealing zone of the SG proximal to the origin of renal and digestive arteries by the creation of fenestration or branched devices or using chimney techniques to preserve the patency of those vessels [8]. However, many challenges remain, such as the proper SG selection, the catheter navigation in tortuous arteries, the geometrical fit between SG and aortic wall, and the alignment of fenestration or side branches for

Abbreviations: AAA, abdominal aortic aneurysm; AMM, anthropomorphic mockup; CBCT, cone beam computed tomography; EVAR, endovascular repair; ILT, intraluminal thrombus; PSI, percutaneous sheath introducers; PVA-C, polyvinyl alcohol cryogel; SG, stent-grafts.

* Corresponding author at: Centre de recherche du Centre hospitalier de l'Université de Montréal (CRCHUM), 900 Rue Saint-Denis, Montréal, Québec H2X 0A9, Canada.
E-mail addresses: gilles.soulez.chum@ssss.gouv.qc.ca, gilles.soulez@umontreal.ca (G. Soulez).

https://doi.org/10.1016/j.medengphy.2019.12.005
1350-4533/

fenestrated, branched grafts or chimney techniques. Current complications of EVAR reflect our inadequate knowledge and experience of the biomechanical interaction between the aortic wall and the medical devices (i.e., SG and catheters). Not only the anatomical feature of AAA, but also the aortic wall degeneration characteristics (i.e., wall stiffening and development of ILT) may all be the contributing factors.

With the blooming development in SG designs (third generation SG, endovascular sealing system [9]) and EVAR approach (endoanchor technique [10] to improve the proximal seal), a better understanding of the biomechanical interaction between the SG and the AAA is becoming critical. However, most biomechanical tests cannot be implemented directly with living human tissue, rendering the vascular mockup an interesting alternative. On the other hand, mockups can be standardized, allowing the experiment to be reproducible, and alleviating experimental limitations due to the cross-species and cross-specimens variability. Of note, most current AAA mockups are developed without considering the surrounding structures [11–13], which may not reflect the realistic behavior of AAA during EVAR. Owing to the diverse morphological characteristics and unclear pathological implications of AAA surrounding tissues [14–18], its biomechanical role has not been studied extensively. Limited studies have demonstrated that the surrounding tissues, especially the abdominal fat and spine, not only constrain AAA deformation but also redistribute wall stress, suggesting the importance of including surrounding tissues in clinical evaluation and treatment planning [19–21]. Hence, an anthropomorphic mockup (AMM) representing the major mechanical, anatomical and pathological characteristics of AAA as well as surrounding tissues is in demand.

Although various synthetic materials have been considered for vascular mockups, especially the silicone which can be easily fabricated in low cost, the selection of materials with desirable mechanical strength and friction property remains limited [22]. Hydrogel has been well known for its biocompatibility, degradation kinetics and mass transfer properties; hence, it is often used for tissue engineering, regenerative medicine and artificial implants [23]. Specifically, the cryogenic polyvinyl alcohol (PVA-C) hydrogel, having excellent compatibility with various medical imaging modalities (ultrasound, CT and MRI), is becoming a popular synthetic material for vascular research. Being a cryogel obtained through specifically designed freezing-thawing cycles, the PVA-C can exhibit non-linear elastic behavior and therefore becomes an excellent candidate to study human soft tissue. By adjusting parameters during PVA-C fabrication, such as the number of the cryogenic cycles, the freezing and thawing rate, the freezing duration and temperature, the mechanical strength of PVA-C can also be tailored to simulate a wide range of biological soft tissues [24–27]. Several studies have also developed PVA-C specimens to investigate the mechanical behavior of human coronary and aortic arteries, with and without diseased characteristics, for example the presence of a lipid pool [28–32]. In addition, the high-water-content property of PVA-C minimizes the surface friction and interfacial energy in contact with biological fluid [33], making this hydrogel an ideal candidate to mimic the interior side of blood vessels.

In the present study, we aimed to develop an AMM of AAA that is mainly composed of PVA-C, which could exhibit the major mechanical, anatomical and pathological characteristics of human AAA and surrounding structures. Such AMM thus provides an essential path to reverse engineer the complex biomechanics of the aortic wall, as well as the interaction with medical devices. EVAR experiments have also been performed with our AMM, and the results highlight the biomechanical effect of surrounding tissues, which is often omitted in simulations of EVAR planning tools.

2. Materials and methods

2.1. AMM design and development

A patient-inspired AAA model generated from a previous work [34] was adopted for the AMM in this study. This model eliminated the geometrical irregularities in patient-specific cases but still well represented the common anatomical and pathological characteristics of human AAA. By varying the parameters during hydrogel fabrication, we tailored the mechanical elasticity of the PVA-C very similar to that of human AAA wall, ILT [35] and abdominal fat [36]. A specific molding-demolding technique with either interconnected or dissolvable molds was applied to reproduce the anatomical and pathogenic features. An air-tight system was designed to maintain the intraluminal and abdominal pressure, and to encase the surrounding tissue such as the abdominal fat and the spine.

2.1.1. Hydrogel preparation

A commercial grade, fully hydrolyzed and soluble polyvinyl alcohol powder (P1763 Sigma-Aldrich) was used. The weight concentration of PVA-C solution was 10%, which allowed a relatively low viscosity to facilitate bubbles release during molding steps. First, the PVA-C powder must be completely dissolved in water at 100 °C, then cooled down and injected into the molds for cryogenic treatment in a temperature-controlled freezer.

Based on our previous experience [28], the cryogenic treatment was designed as follows: each cycle was first frozen at a rate of 0.333 °C/min to −20 °C and rested for two hours, then thawed at a rate of 0.08 °C/min to 10 °C and rested for another two hours. A thermal couple was inserted at the center of the molds to monitor temperature variations. Numbers of studies have demonstrated that repeated thermal cycling of PVA-C can increase the crystallinity in the hydrogel, thereby increasing its elastic modulus [37–42]. Therefore, PVA-C specimens with the same cryogenic treatment but different number of cycles were fabricated to determine the optimal number of cycles for each application (stiffen aortic wall, ILT and abdominal fat).

2.1.2. Mold fabrication

Due to the complexity in our model geometry, rapid prototyping technology (P430, Dimension Elite, Stratasys, print in acrylonitrile butadiene styrene) was ideal for mold fabrication. However, an efficient and equilibrium heat transfer through the molds was critical to ensure proper temperature control. Molds were therefore designed in a uniform thickness of 2 mm to facilitate heat transfer. Once the molds were fabricated, surface treatments were needed to ensure the surface smoothness so that bubble formation during PVA curing can be avoided, without affecting much of the original mold thickness (final mold thickness 2 ± 0.1 mm).

2.1.3. Realistic anatomy

In order to create a tubular and bifurcating vessel in one piece, the final mold design consisted of a detachable inner mold, the outer molds that can split in two halves, and three caps at all ends to properly seal and align the inner and outer molds. For human AAAs, Raghavan et al. have reported the wall thickness varied from 0.23 mm to 4.26 mm [43]. A uniform thickness of 2 mm along the AAA, as the mean of those values, has been commonly adopted in AAA computational models [44–47] and thus, also considered in this study. As such, the space between the inner and outer molds was designed to remain at 2 mm. To combine PVA-C parts with different mechanical strength, a multi-layer molding technique (Fig. 1) along with a specific molding sequence during PVA-C fabrication was applied. Specifically, after three cycles of cryogenic treatment, the second set of outer molds (same dimension but without ILT extrusion) was used, so that PVA-C solution

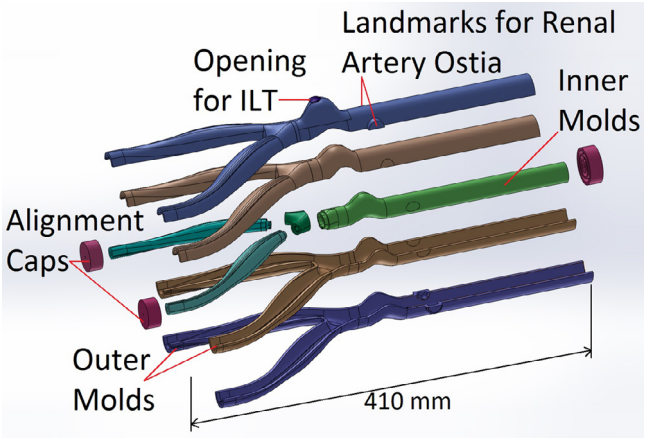

Fig. 1. Multi-layer molds for the addition of ILT.

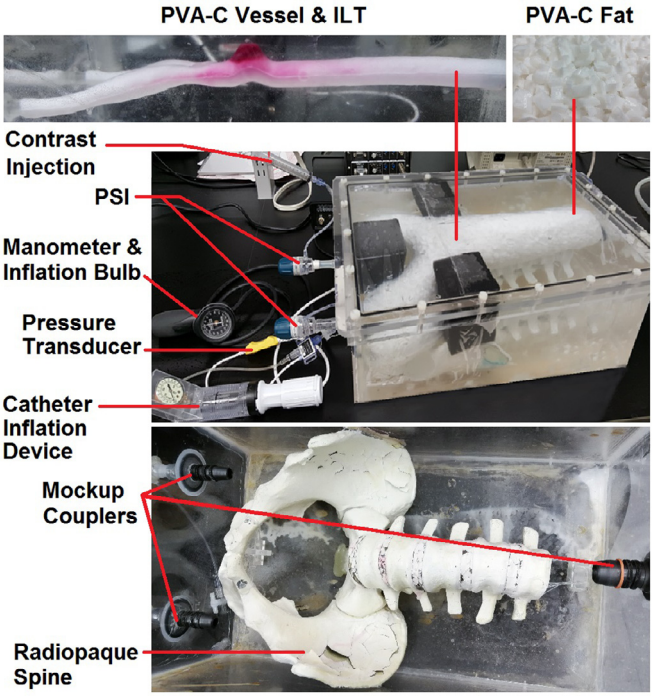

Fig. 2. Anthropomorphic system to encase PVA-C vessel with ILT (red ink added to visually distinguish ILT from aortic wall), surrounding PVA-C fat, radiopaque spine, and to maintain abdominal and intraluminal pressure.

could be injected through a small opening to the site of ILT, then together cured for five more cycles to create an ILT attaching to the AAA wall. As renal artery ostia are the important landmarks during EVAR, two glass beads were embedded into the PVA-C wall at those locations.

2.1.4. Anthropomorphic system

In order to represent the major pathological characteristics of AAA, some surrounding tissues as well as the intraluminal and abdominal pressure were included in this AMM (Fig. 2). A thick layer of PVA-C fat cubes (3–6 cm) was laid over the whole vessel to mimic the surrounding fat; it was gently wrapped by a customized cotton-mesh envelop without compressing the vessel. An air-tight plexiglass container was developed to encase the vessel along with abdominal fat and a radiopaque spine (LSS-10, AMS Labs Inc.), to allow for optimal exposure with various imaging techniques. The spine was glued and attached firmly at the bottom to eliminate dislocation during EVAR. The proximal and distal ends of vessel were carefully slipped over the mockup couplers having deep grooves, so that the vessel could be fastened by cable ties to prevent leakage. At distal end, these couplers were also attached to the percutaneous sheath introducers (PSI) to provide a hemostatic seal and the access of catheters during EVAR. The port from one PSI was used to inject contrast agent, whereas from another PSI was connected to a balloon catheter inflation device via a pressure transducer (Vivitro Labs Inc.), to monitor the intraluminal pressure at 100 mmHg (ViviTest 4.0). The abdominal pressure inside this system was maintained manually at 12 mmHg [48], by a dial manometer along with inflation bulb.

2.2. Mechanical properties

2.2.1. Tensile tests

PVA specimens with two to ten thermal cycles were tested and compared with soft tissue values from literatures. Uniaxial tensile tests were carried out using a mechanical tester (Bose, Enduratec ELF 3200). All samples were cut into rectangular strips of 40 mm by 10 mm with a uniform thickness of 2 mm (to mimic averaged AAA wall). Immediately upon fabrication, all samples were stored in water at 5 °C, and then equilibrated to room temperature (~24 °C) an hour prior to mechanical testing. Two clamps with saw-tooth surface were employed to provide firm gripping of the samples during stretching. According to our previous study [28], six preconditioning cycles were performed prior to the actual test of a maximum 50% extension at a constant speed of 0.1 mm/s. Three samples were repeated for each set of cryogenic treatment.

The applied force $\boldsymbol{F}$ and displacement $\boldsymbol{\Delta l}$ were recorded and the stress–strain curve obtained by calculating the Cauchy stress $\boldsymbol{\sigma}$ and engineering strain $\boldsymbol{\varepsilon}$ as follows ($\boldsymbol{A}$: current cross-section area; $\boldsymbol{L}$: initial length).

$$\sigma = \frac{F}{A}\ ,\ \varepsilon = \frac{\Delta l}{L}$$

Assuming incompressibility, the sample volume $\boldsymbol{v}$ at any given strain should be conserved. Hence, $\boldsymbol{A}$ and the stress at any given strain $\boldsymbol{\sigma}$ was adjusted as follows ($\boldsymbol{A_0}$: initial cross-section area).

$$A = \frac{v}{L+\Delta l} = \frac{A_0 \times L}{L+\Delta l} = \frac{A_0}{1+\varepsilon}$$

$$\sigma = \frac{F}{A_0} \times (1+\varepsilon)$$

Since some of our measurements involved larger strain values, the engineering strain ε mentioned above may not reflect the large strain behavior. Hence, Green strain tensor was used, where the only non-zero component $\boldsymbol{E_{xx}}$ for uniaxial tension was calculated as follows (assuming tension along x-direction).

$$E_{xx} = \frac{\partial u}{\partial x} + \frac{1}{2}\left(\frac{\partial u}{\partial x}\right)^2 = \frac{\Delta l}{L} + \frac{1}{2}\left(\frac{\Delta l}{L}\right)^2 = \varepsilon + \frac{\varepsilon^2}{2}$$

2.2.2. Friction tests

The goal was to assess the friction behavior of our AMM interacting with EVAR catheters, especially the polymeric sheath with a hydrophilic coating, and then compare the results with that of human aortic tissue and the tissue-mimicking silicone.

The tests were carried out using a Biomomentum Mach 1 v500csst with the experimental set-up as illustrated in Figure 3. The catheter sheath was cut and flattened into a rectangular strip, then gently mounted to the bottom of a shaft (15 mm × 15 mm contact area) connecting to the load cell. With the high-precision multi-axial load cell, friction forces $\mathbf{F_T}$ were measured while a range of normal loads $\mathbf{F_N}$ were applied: 0.1 N (equivalent to force during smooth catheter navigation), 1 N, 2 N and 3 N (equivalent to force during SG deployment) [49]. Three types of specimens were tested: PVA-C mimicking human AAA wall (number of

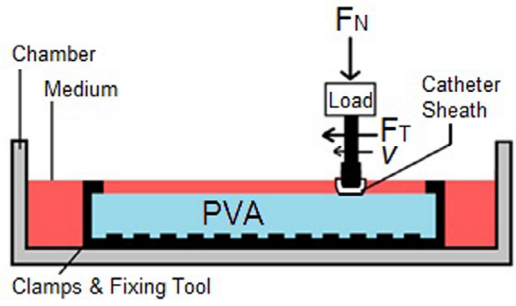

Fig. 3. Schematic illustration of friction test experimental setup.

cryogenic cycles determined after tensile tests), three kinds of silicone commonly used for vascular mockups (Sylgard 184 silicone elastomer from Dow Corning, Mold Max^{TM} 20 and Mold Max^{TM} XLS^{TM} II from Smooth-On Inc.) [50–53], and diseased human AAA tissue (anterior abdominal aortic region, obtained following aortic reconstruction surgeries at Montreal Heart Institute with ethical approval, refrigerated in phosphate buffered saline and tested within 24 h). Water was filled up to the contact surface and all experiments were conducted at room temperature (~24 °C).

With the aim of obtaining the Stribeck curves (friction coefficient vs. sliding velocity) to better describe the friction behavior, a set of constant sliding speeds were tested for a sliding distance of 80 mm: from 0.5 mm/s to 50 mm/s, with an increment of 5 mm/s.

2.3. EVAR experiment

EVAR experiments were performed using our AMMs by an interventional specialist in a realistic clinical set-up (Artis-Q, Siemens Healthineers, Forccheim, Germany). One shot and cone beam CT (CBCT) scans were acquired during every stage of EVAR (6 s C-arm spin, 0.47 × 0.47 × 0.47 mm voxels and 24 × 24 × 18.5 cm acquisition volume). 3D models of the lumen and SG were also reconstructed by thresholding technique (lumen < 250 HU; SG > 1000 HU [54]) and snake evolution with ITK-SNAP (version 3.6.0) to verify proper deployments.

While keeping the abdominal pressure stable, the vessel expansion along with a gradual increase of luminal pressure (80 mmHg to 160 mmHg) was also recorded by CBCT scans prior to EVAR experiments. For each set of AMM, three zenith SG (TFFB-24-82-ZT, ZSLE-20-56-ZT, ZSLE-24-74-ZT, Cook Medical, Bloomington, IN) were deployed over a Lunderquist Wire (Cook Medical). Note that, for each experiment, new SGs were deployed in a new PVA-C mockup in order to prevent any unexpected device damages while retrieving SGs, as well as damages on the aortic wall due to anchoring hooks from SGs. The main body and the right iliac artery were inserted through the right limb of the AMM whereas the left iliac artery was inserted through the left limb of the AMM. One shot acquisitions and fluoroscopy scenes were saved during the insertion of guide wires, delivery devices and SG deployment. Similarly, CBCT acquisitions were acquired both before and after these procedural steps.

To study the effect of surrounding tissue, two sets of AMMs were considered for the same EVAR treatments: one with surrounding abdominal fat and the other one without it. The centerline of lumen along the aorta at every stage was computed by the Vascular Modeling Toolkit (version 1.4.0), and the displacement of centerline was obtained from the Hausdorff distance calculated by MATLAB (version R2018a). In order to confirm our experimental observations with clinical data, three anonymous EVAR patients with AAA characteristics similar to our AMM (almost no calcification, small eccentric thrombus and 0.18–0.39 iliac tortuosity, whereas AMM has 0.22 iliac tortuosity) were selected from our recent patient database (with ethical approval). Similar centerline extractions were repeated for each patient, and the centerline displacements at different EVAR stages were compared to relevant values from AMM experiments.

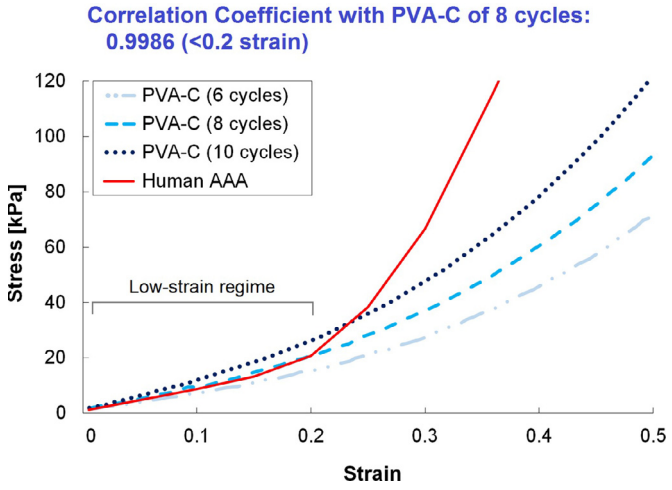

Fig. 4. Stress–strain behavior of PVA-C gel with 6, 8 and 10 cryogenic cycles compared to that of human AAA tissue from literature.

3. Results

3.1. Biomechanically realistic

With the results of uniaxial tensile tests, the numbers of cryogenic cycles for specific applications (AAA wall, ILT and abdominal fat) were determined. Standard deviations for our experimental results were very small and hence not shown in the following plots.

The elastic behavior of PVA-C cured with 6, 8 and 10 cryogenic cycles were compared to that of human AAA wall [55]. An excellent agreement between eight-cycle PVA-C and human tissue was observed up till 20% strain (Fig. 4), indicating eight cryogenic cycles as the most suitable treatment to mimic AAA wall.

For human ILT, the stress–strain behavior of our PVA-C with 4 and 5 cryogenic cycles was found to be closest to the human values reported in the literature [56]. Assuming the ILT to be homogeneous and isotropic, results suggested that PVA-C with five cycles could better represent the averaged stress–strain values from literature (Fig. 5) and thus, was selected to mimic human ILT.

Comparing the uniaxial tensile stress of PVA-C with two cryogenic cycles to that of human abdominal fat [36], one should notice that the stress–strain curve of this PVA-C lies between the curves of human fat in both longitudinal and circumferential directions (Fig. 6), confirming it to be the optimal selection to approximate human abdominal fat.

For friction behavior between the catheter sheath and PVA-C, silicone or human aortic tissue under a normal load of 0.1 N, results clearly indicated that friction coefficients of PVA-C at various sliding velocity were similar to those of human AAA wall, whereas the tissue-mimicking silicone carried much higher friction coefficients (Fig. 7, left). Hence, PVA-C was confirmed to be an ideal candidate for mockups to investigate the biomechanical interaction between human vessel and endovascular devices. In addition, the Stribeck curves (Fig. 7, right) describing the relationships between sliding velocities and friction coefficients of PVA-C, as well as human aortic tissue, revealed that friction coefficients generally decreased as sliding velocities increased (≥ 5 mm/s). This was commonly observed for all normal loads except for 0.1 N which shifted

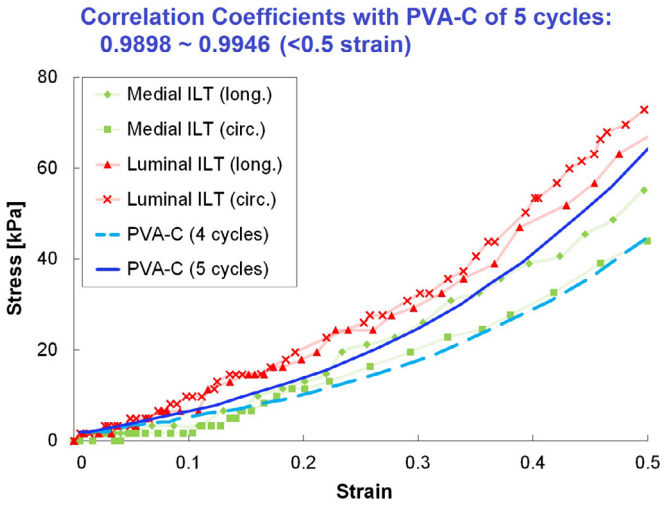

Fig. 5. Stress–strain behavior of PVA-C gel with 4 and 5 cryogenic cycles compared to that of human ILT (long.: longitudinal direction; circ.: circumferential direction) from literature.

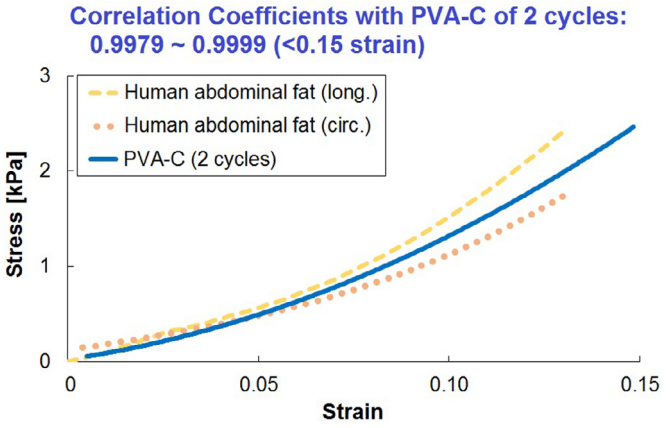

Fig. 6. Stress–strain behavior of PVA-C gel with 2 cryogenic cycles compared to that of human abdominal fat (long.: longitudinal direction; circ.: circumferential direction) from literature.

drastically upwards in both cases, potential cause will be discussed later.

3.2. Anatomically and pathologically realistic

The PVA-C vessel with bifurcating iliac arteries has been fabricated using detachable molds with inter-locking system (Fig. 1). The relatively softer ILT (Fig. 2) has also been created through fewer cycles of cryogenic treatment and cross-linked firmly to the vessel wall through the multi-layer molding technique. Having assembled the vessel to the anthropomorphic system with the static luminal and abdominal pressure, no leak was observed through the vessel wall; in addition, no pressure change was recorded in the vessel and the surrounding space. To conclude, an AMM representing the major anatomical and pathological characteristics of AAA has been successfully developed using our proposed method.

3.3. Mockup EVAR experiment

To mimic a cardiac cycle with the intraluminal pressure varied between 80 mmHg (diastolic) and 160 mmHg (systolic), a pressure gradient of 80 mmHg was applied. In the case with surrounding fat, vessel expansion was minimal (1.8% in diameter and 3.4% in area) with an 0.4 overall distensibility (area change/pressure gradient, unit in 10^{-5} Pa^{-1}); whereas in the case without surrounding fat, significant vessel expansion (9.4% in diameter and 21% in area) with a 2.1 overall distensibility was observed (Fig. 8).

While performing EVAR using our AMM without surrounding fat, the vessel deformation during SG deployment was more vigorous than what we could observe clinically. By comparing the aortic centerlines at different navigation and deployment stages to the one at initial stage, we observed the maximum displacement occurred at the deployment stage with a Hausdorff distance of 29.6 mm (Fig. 9). While the surrounding abdominal fat was present, the range of motion during EVAR appeared within the ex-

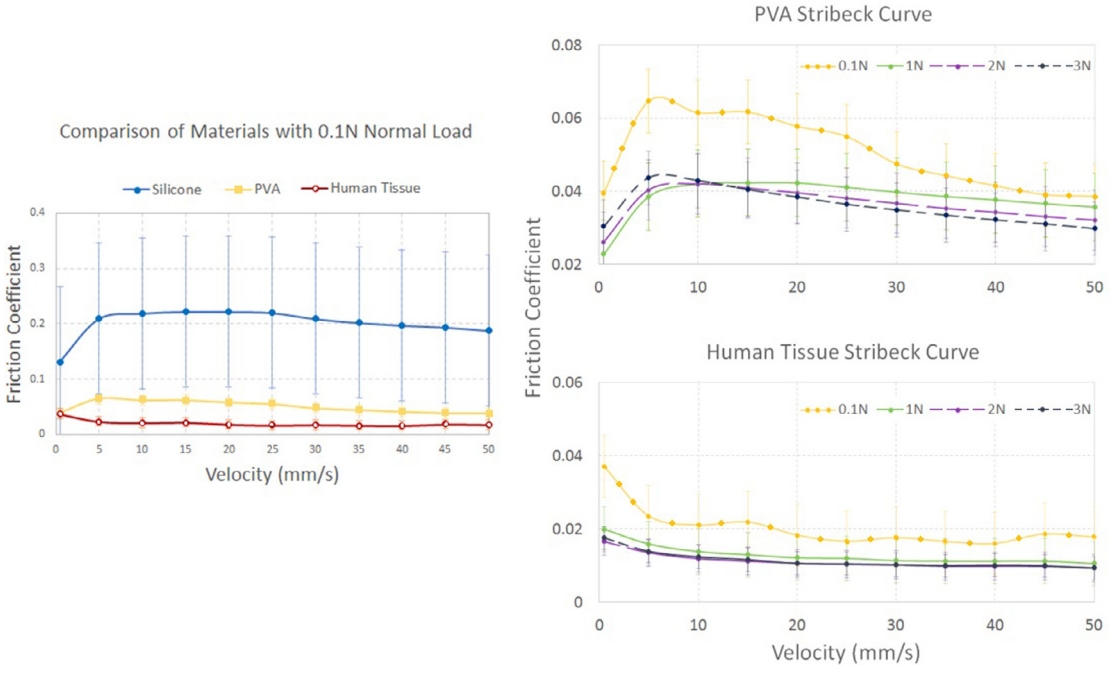

Fig. 7. Comparison of friction coefficients of different materials with 0.1 N normal load (left); comparison of Stribeck curves of PVA-C and human aortic tissue (right).

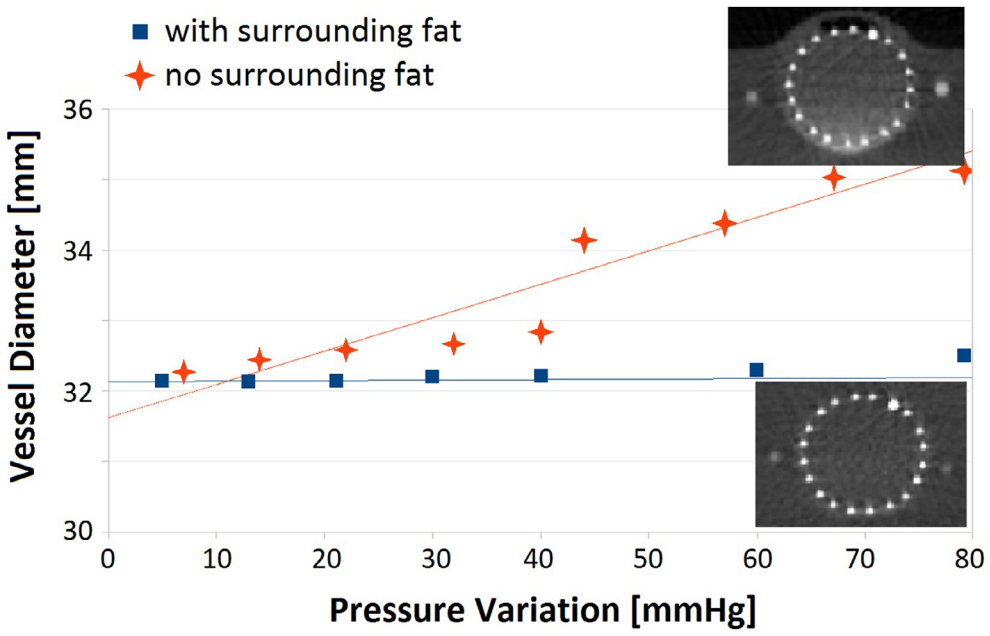

Fig. 8. Vessel expansion with intraluminal pressure. Two dots outside the lumen indicate the location of renal artery ostia.

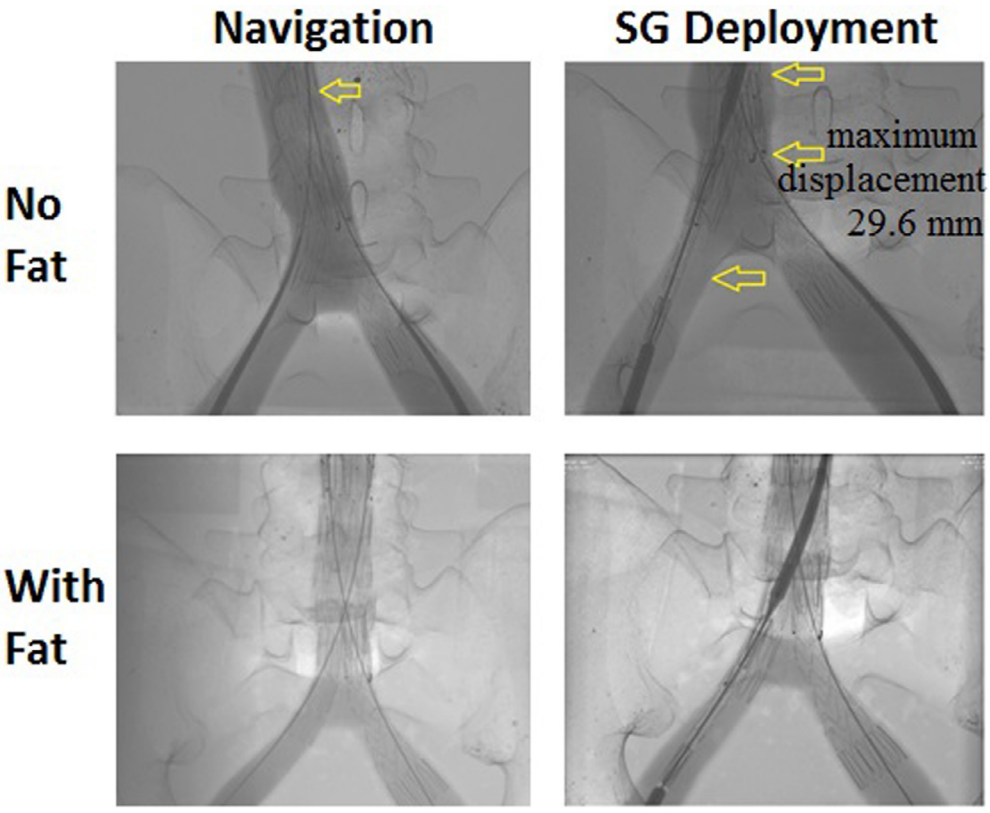

Fig. 9. Vessel displacement and deformation during EVAR navigation and SG deployment stages.

pectation of our medical specialists. The maximum centerline displacement was also found at deployment stage with a Hausdorff distance of 6.7 mm, significantly smaller than the case without surrounding fat. While applying the same method to clinical data, the maximum centerline displacements for all selected patients were found during SG deployment as well, with the Hausdorff distances being 6.8 mm, 7.2 mm and 12.3 mm. Hence, the aortic centerline displacements during EVAR in the case of AMM with surrounding tissue better agree with the range of aortic centerline deviation observed clinically.

4. Discussion

In general, tensile test results matched well with our previous observations in a more detailed study for PVA-C mechanical characterization [28], confirming the reproducibility of the desired

elasticity in PVA-C. For the AAA wall, although the elastic modulus of human tissue increases much faster after 25% strain, the stress–strain curve of PVA with eight cycles displays an excellent match with human AAA tissue under 20% strain. Keeping in mind that the objective in this study is to develop an AMM to investigate the effects of EVAR, and a 10% to 20% oversizing is the standard for SG selection [52], which implies a maximum of 15% strain in the AAA wall along circumferential direction. Therefore, PVA-C with eight cycles of cryogenic treatment could sufficiently approximate the mechanical response of human AAA wall in this study. For the ILT, although it has been well characterized as an inhomogeneous material consisting of multiple layers with variable stiffness and thickness, reproducing these microscopic details may not result in significantly different AAA responses during EVAR. Similarly, the abdominal fat was assumed to be isotropic in this study, regardless of its more complex nature, because it was considered here to simply provide an adequate support and resistance during EVAR. Thus, PVA-C with five and two cryogenic cycles could best mimic the averaged compliance of ILT and human abdominal fat respectively.

To date, most vascular mockups have been developed to address a single or few parameters in questions. For example: transparent but relatively rigid mockups made of polyurethane or epoxy resin for hemodynamics studies [12,57]; compliant mockups made of mold-casted silicone [58–60] or hydrogel [29,61,62] for medical imaging and computational validations, but often in simple geometry; 3D-printed flexible mockups in complex geometry for medical trainings and benchmark testing, but with less desirable mechanical properties [13,63]. On the other hand, surrounding structures and pathological characteristics are still rarely considered due to the complexity in mockup development. This study presents an AMM that reproduces not only anatomical characteristics, but also realistic mechanical behavior, specifically the elasticity and friction, of major AAA components (aortic wall and ILT) and surrounding structures (abdominal fat and spine). As friction is becoming a main concern in Benchmark testing for medical device navigation [64], this AMM offers tremendous value to ameliorate the current design of EVAR catheters. By incorporating major surrounding structures, the luminal and abdominal pressure into this AMM, we provide by far the most sophisticated and comprehensive in-vitro model to study the biomechanical interaction between AAA and medical devices.

From our mock EVAR experiments, the biomechanical effects of surrounding structures, especially the surrounding fat, was elucidated. First, it helped to reduce instantaneous vessel expansion under luminal pressure, providing more realistic AAA responses compared to in vivo data (0.31–1.27 10^{-5} Pa^{-1} distensibility and 0.3%–4.8% area change over a cardiac cycle) [65,66]. The importance to consider zero-pressure geometry in simplified simulations without surrounding tissues was also underlined. Second, it helped to significantly resist forces associated with catheter navigation and SG deployment during EVAR. The difference in centerline deviations implies a dampening effect of the surrounding fat when an external force is introduced by catheter or SG, which provides an important framework to account for the interactions with those endovascular devices. Of note, surrounding tissues are still ignored or simplified as an artificial boundary condition in most studies of AAA biomechanics, especially when simulating the interaction with medical devices during EVAR [67,68], which can impact the predictive capability [69,70]. Our results therefore provide an insight to refine existing numerical models for more realistic and accurate prediction in EVAR outcomes.

Another advantage of this AMM is the durability and material cost. Based on our laboratory experience, if all PVA-C components are stored in cool and clean water without fungi contamination (anti-algae aquarium product may be used) and direct sun light, the structural integrity as well as mechanical properties can be well preserved for at least a year, whereas the long-term (>1 year) mechanical properties remain to be assessed. As to fabricate this AMM, the PVA powder used for the vessel, ILT and surrounding fat together costed under $100; whereas the material cost for molds was around $200 and for the anthropomorphic system (excluding pressure transducer and controller) was around $400, in which many components can be reused for different AAA geometries. With the described methodology, it will only take a week to fabricate each hydrogel mockup, and few weeks to develop the reusable molds and the anthropomorphic system. Nevertheless, the success rate of PVA-C mockup fabrication, especially for such a delicate AMM, greatly depends on the skills and experience of the developer, mainly due to the number of challenges discussed as follows.

The biggest challenge in mold design and fabrication is the inter-locking system of the detachable inner mold. It should not only address the aneurismal and bifurcating characteristics of AAA, but also facilitate the demolding process. Although PVA-C is deformable, minor damage can be incurred while removing the inner mold and can cause hydrogel tearing under pressure. Hence, sharp edges and corners were avoided in each inter-locking component. Besides, the connections between components were designed in a laminated manner to prevent leaking of the PVA solution, as well as bending or deflection along the assembled mold. Another challenge is the printing orientation, especially for the inter-locking system. As one of the limitations in FDM (fused deposition modeling) printing technology, the finished product is often weaker along the vertical direction. Thus, the printing orientation was carefully selected to maximize the strength and durability of molds, especially at the connection tips of inner molds.

During PVA-C fabrication, molds with rough surface finish could be an issue with the current 3D printing technology. A tiny bump on the mold surface may easily trap bubbles between the inner and outer molds, resulting in voids inside the thin PVA-C wall and thus, higher risk of wall rupture under luminal pressure. Therefore, detailed post-processing such as manual sanding, acetone-treatment and thin varnish coating were necessary. As a result of the thin molds with smooth surface, the thickness of final AMM aortic wall, after eight cryogenic cycles, remained unchanged (1.98 ± 0.02 mm).

For the friction tests, some limitations exit in the current study. First, measurements with silicone under normal load greater than 0.1 N was not possible, because the friction force became too high and exceeded the limit of load cell. Nevertheless, 0.1 N is too small to represent the navigation force in the case of tortuous iliac arteries, our observation thus confirms that tissue-mimicking silicone could not sufficiently mimic the frictional behavior of human vessel. Second, all Stribeck curves of 0.1 N normal load shift drastically upwards. This indicates that the friction between the aortic wall and the catheter at low normal load was significantly affected by the surface flatness; it may also be influenced by the sensitivity of a high-precision load cell, which remains to be clarified in future. Third, the range of sliding velocity limited us from having a complete description of the PVA-C frictional behavior at both elastic friction and hydrodynamic lubrication regions. Stribeck curves from our results suggest that both materials are only under elastic friction [71], whereas hydrodynamic lubrication dominated by the lubricating liquid has never been reached in our experiments due to the limitation in sliding velocity amplitude. Nevertheless, according to the comments and experience from endovascular specialists in our team, the sliding speeds in this study cover far beyond the catheter navigation speed in clinical practice.

Finally, as one of the major characteristics in AAA wall degeneration, calcification at the aortic wall may directly affect the interaction with endovascular devices. Thus, including calcification in our

AMM would be of great interest. Moreover, extending the current work into patient-specific models, especially with tortuous iliac arteries would be highly desired.

Despite the current limitations and future improvements, being biomechanically, anatomically and pathologically realistic, this AMM can provide an excellent in-vitro environment for numerical model validation, medical device evaluation, academic demonstration and medical training. As this paper only presents the experimental study of a project for which the ultimate goal is to develop a virtual planning tool for EVAR, our results will be combined with clinical data to refine existing numerical simulations [70] and eventually, to improve procedure planning, outcomes prediction, effectiveness and durability of EVAR procedures.

5. Conclusions

The current work is the first in which a PVA-C based anthropomorphic perfused mockup for AAA is developed. Specifically, our AMM allows to reproduce realistic deformation responses, frictional behavior, anatomical and diseased characteristics observed with AAAs. To our knowledge, the effects of surrounding tissues have not been addressed in previous studies of AAA. Using this AMM, we evaluated the biomechanical interaction between AAA and medical devices during EVAR, with and without the surrounding fat. Our results highlight the indispensable role of surrounding tissues, not only the spine but also the abdominal fat, as to account for realistic interactions with endovascular devices.

Declaration of Competing Interest

None.

Ethical approval

The image data used in this article was acquired with the authorization of the Research Center Ethics Board of Centre Hospitalier de l'Université de Montréal.

The human tissue for friction measurements was collected with the informed consent and ethical approval at the Montreal Heart Institute.

Acknowledgments

We acknowledge the support of the Natural Sciences and Engineering Research Council of Canada (CRDPJ 460903-13 and RDCPJ 510049-17), MEDTEQ, CAE Healthcare, and Siemens Healthcare Limited.

References

[1] Karthikesalingam A, Holt PJ, Vidal-Diez A, Ozdemir BA, Poloniecki JD, Hinchliffe RJ, et al. Mortality from ruptured abdominal aortic aneurysms: clinical lessons from a comparison of outcomes in England and the USA. The Lancet 2014;383:963–9. doi:10.1016/S0140-6736(14)60109-4.

[2] Beck AW, Goodney PP, Nolan BW, Likosky DS, Eldrup-Jorgensen J, Cronenwett JL. Predicting 1-year mortality after elective abdominal aortic aneurysm repair. J Vasc Surg 2009;49:838–44. doi:10.1016/j.jvs.2008.10.067.

[3] Greenhalgh RM, Brown LC, Powel JT, Thompson SG, Epstein D, Sculpher MJ. Endovascular versus open repair of abdominal aortic aneurysm. N Engl J Med 2010;362:1863–71. doi:10.1056/NEJMoa0909305.

[4] Acosta S, Lindblad B, Zdanowski Z. Predictors for outcome after open and endovascular repair of ruptured abdominal aortic aneurysms. Eur J Vasc Endovasc Surg 2007;33:277–84. doi:10.1016/j.ejvs.2006.09.017.

[5] Schermerhorn ML, Buck DB, O'Malley AJ, Curran T, McCallum JC, Darling J, et al. Long-term outcomes of abdominal aortic aneurysm in the medicare population. N Engl J Med 2015;373:328–38. doi:10.1056/NEJMoa1405778.

[6] Arnaoutakis DJ, Zammert M, Karthikesalingam A, Belkin M. Endovascular repair of abdominal aortic aneurysms. Best Pract Res Clin Anaesthesiol 2016;30:331–40. doi:10.1016/j.bpa.2016.05.004.

[7] Herman CR, Charbonneau P, Hongku K, Dubois L, Hossain S, Lee K, et al. Any nonadherence to instructions for use predicts graft-related adverse events in patients undergoing elective endovascular aneurysm repair. J Vasc Surg 2018;67:126–33. doi:10.1016/j.jvs.2017.05.095.

[8] Kansagra K, Kang J, Taon M-C, Ganguli S, Gandhi R, Vatakencherry G, et al. Advanced endografting techniques: snorkels, chimneys, periscopes, fenestrations, and branched endografts. Cardiovasc Diagn Ther 2018;8:S175–83. doi:10.21037/cdt.2017.08.17.

[9] Carpenter JP, Cuff R, Buckley C, Healey C, Hussain S, Reijnen MMPJ, et al. One-year pivotal trial outcomes of the Nellix system for endovascular aneurysm sealing. J Vasc Surg 2017;65:330–336.e4. doi:10.1016/j.jvs.2016.09.024.

[10] Galiñanes EL, Hernandez E, Krajcer Z. Preliminary results of adjunctive use of endoanchors in the treatment of short neck and pararenal abdominal aortic aneurysms. Catheter Cardiovasc Interv 2016;87:E154–9. doi:10.1002/ccd.26351.

[11] Cloutier G, Soulez G, Qanadli SD, Teppaz P, Allard L, Qin Z, et al. A multimodality vascular imaging phantom with fiducial markers visible in DSA, CTA, MRA, and ultrasound. Med Phys 2004;31:1424–33. doi:10.1118/1.1739300.

[12] Allard L, Soulez G, Chayer B, Qin Z, Roy D, Cloutier G. A multimodality vascular imaging phantom of an abdominal aortic aneurysm with a visible thrombus. Med Phys 2013;40:063701. doi:10.1118/1.4803497.

[13] Meess KM, Izzo RL, Dryjski ML, Curl RE, Harris LM, Springer M, et al. 3D printed abdominal aortic aneurysm phantom for image guided surgical planning with a patient specific fenestrated endovascular graft system. Proc SPIE – Int Soc Opt Eng 2017;10138. doi:10.1117/12.2253902.

[14] Thanassoulis G, Massaro JM, Corsini E, Rogers I, Schlett CL, Meigs JB, et al. Periaortic adipose tissue and aortic dimensions in the Framingham Heart Study. J Am Heart Assoc 2012;1:e000885. doi:10.1161/JAHA.112.000885.

[15] Padilla J, Jenkins NT, Vieira-Potter VJ, Laughlin MH. Divergent phenotype of rat thoracic and abdominal perivascular adipose tissues. Am J Physiol Regul Integr Comp Physiol 2013;304:R543–52. doi:10.1152/ajpregu.00567.2012.

[16] Horimatsu T, Kim HW, Weintraub NL. The role of perivascular adipose tissue in non-atherosclerotic vascular disease. Front Physiol 2017;8. doi:10.3389/fphys.2017.00969.

[17] Szasz T, Clinton Webb R. Perivascular adipose tissue: more than just structural support. Clin Sci Lond Engl 2012;122:1–12 1979. doi:10.1042/CS20110151.

[18] Harvey Wolinsky, Seymour Glagov. Comparison of abdominal and thoracic aortic medial structure in mammals. Circ Res 1969;25:677–86. doi:10.1161/01.RES.25.6.677.

[19] Villacorta L, Chang L. The role of perivascular adipose tissue in vasoconstriction, arterial stiffness, and aneurysm. Horm Mol Biol Clin Investig 2015;21:137–47. doi:10.1515/hmbci-2014-0048.

[20] Kim J, Peruski B, Hunley C, Kwon S, Baek S. Influence of surrounding tissues on biomechanics of aortic wall. Int J Exp Comput Biomech 2013;2:105–17. doi:10.1504/IJECB.2013.056516.

[21] Kwon ST, Burek W, Dupay AC, Farsad M, Baek S, Park E-A, et al. Interaction of expanding abdominal aortic aneurysm with surrounding tissue: retrospective CT image studies. J Nat Sci 2015;1:e150.

[22] Sadasivan C, Lieber BB, Woo HH. Physical simulators and replicators in endovascular neurosurgery training. In: Alaraj A, editor. Comprehensive healthcare simulation: neurosurgery. Cham: Springer International Publishing; 2018. p. 29–45. doi:10.1007/978-3-319-75583-0_3.

[23] Ashton Acton Q. Polyethylene glycols—advances in research and application. 2013th ed. ScholarlyEditions; 2013.

[24] Stauffer SR, Peppast NA. Poly(vinyl alcohol) hydrogels prepared by freezing-thawing cyclic processing. Polymer 1992;33:3932–6. doi:10.1016/0032-3861(92)90385-A.

[25] Ku D.N., Braddon L.G., Wootton D.M., inventor; Georgia Tech Research Corp, assignee. Poly(vinyl alcohol) cryogel. United States patent US 5981826A. 1999.

[26] Lozinsky VI, Damshkaln LG. Study of cryostructuration of polymer systems. XVII. Poly(vinyl alcohol) cryogels: dynamics of the cryotropic gel formation. J Appl Polym Sci 2000;77:2017–23. doi:10.1002/1097-4628(20000829)77:9⟨2017::AID-APP18⟩3.0.CO;2-6.

[27] Wan WK, Campbell G, Zhang ZF, Hui AJ, Boughner DR. Optimizing the tensile properties of polyvinyl alcohol hydrogel for the construction of a bioprosthetic heart valve stent. J Biomed Mater Res 2002;63:854–61. doi:10.1002/jbm.10333.

[28] Pazos V, Mongrain R, Tardif JC. Polyvinyl alcohol cryogel: optimizing the parameters of cryogenic treatment using hyperelastic models. J Mech Behav Biomed Mater 2009;2:542–9. doi:10.1016/j.jmbbm.2009.01.003.

[29] Pazos V, Mongrain R, Tardif JC. Deformable mock stenotic artery with a lipid pool. J Biomech Eng 2010;132:034501. doi:10.1115/1.4000937.

[30] Pazos V, Mongrain R, Tardif J-C. Mechanical characterization of atherosclerotic arteries using finite-element modeling: feasibility study on mock arteries. IEEE Trans Biomed Eng 2010;57:1520–8. doi:10.1109/TBME.2010.2041001.

[31] Reiter S, Mongrain R, Abdelali M, Tardif J-C. Medical applications of poly(vinyl alcohol) cryogels. In: Kalia S, Fu S-Y, editors. Polymers at cryogenic temperatures. Springer Berlin Heidelberg; 2013. p. 147–59.

[32] Le Floc'h S, Cloutier G, Finet G, Tracqui P, Pettigrew RI, Ohayon J. On the potential of a new IVUS elasticity modulus imaging approach for detecting vulnerable atherosclerotic coronary plaques:in vitrovessel phantom study. Phys Med Biol 2010;55:5701–21. doi:10.1088/0031-9155/55/19/006.

[33] Ohta M, Handa A, Iwata H, Rüfenacht DA, Tsutsumi S. Poly-vinyl alcohol hydrogel vascular models for in vitro aneurysm simulations: the key to low friction surfaces. Technol Health Care 2004;12:225–33.

[34] Roy D. Mechanical simulation of the endovascular repair of abdominal aortic aneurysms. Montréal (QC): Université de Montréal; 2015.

[35] Roy D, Kauffmann C, Delorme S, Lerouge S, Cloutier G, Soulez G. A literature review of the numerical analysis of abdominal aortic aneurysms treated with endovascular stent grafts. Comput Math Methods Med 2012;2012. doi:10.1155/2012/820389.
[36] Sommer G, Eder M, Kovacs L, Pathak H, Bonitz L, Mueller C, et al. Multiaxial mechanical properties and constitutive modeling of human adipose tissue: a basis for preoperative simulations in plastic and reconstructive surgery. Acta Biomater 2013;9:9036–48. doi:10.1016/j.actbio.2013.06.011.
[37] Watase M, Nishinari K, Nambu M. Anomalous increase of the elastic modulus of frozen poly(vinyl alcohol) gels. CryoLetters 1983;4:197–200.
[38] Watase M, Nishinari K. Rheological and DSC changes in poly(vinyl alcohol) gels induced by immersion in water. J Polym Sci Polym Phys Ed 1985;23:1803–11. doi:10.1002/pol.1985.180230906.
[39] Watase M, Nishinari K. Large deformation of hydrogels of poly(vinyl alcohol), agarose and kappa-carrageenan. Makromol Chem 1985;186:1081–6. doi:10.1002/macp.1985.021860517.
[40] Watase M, Nishinari K. Thermal and rheological properties of poly(vinyl alcohol) hydrogels prepared by repeated cycles of freezing and thawing. Makromol Chem 2003;189:871–80. doi:10.1002/macp.1988.021890419.
[41] Watase M, Nishinari K. Effect of the degree of saponification on the rheological and thermal properties of poly(vinyl alcohol) gels. Makromol Chem 1989;190:155–63. doi:10.1002/macp.1989.021900117.
[42] Peppas NA, Stauffer SR. Reinforced uncrosslinked poly (vinyl alcohol) gels produced by cyclic freezing-thawing processes: a short review. J Controlled Release 1991;16:305–10. doi:10.1016/0168-3659(91)90007-Z.
[43] Raghavan ML, Kratzberg J, Castro de Tolosa EM, Hanaoka MM, Walker P, da Silva ES. Regional distribution of wall thickness and failure properties of human abdominal aortic aneurysm. J Biomech 2006;39:3010–16. doi:10.1016/j.jbiomech.2005.10.021.
[44] Heng MS, Fagan MJ, Collier JW, Desai G, McCollum PT, Chetter IC. Peak wall stress measurement in elective and acute abdominal aortic aneurysms. J Vasc Surg 2008;47:17–22. doi:10.1016/j.jvs.2007.09.002.
[45] Metaxa E, Tzirakis K, Kontopodis N, Ioannou CV, Papaharilaou Y. Correlation of intraluminal thrombus deposition, biomechanics, and hemodynamics with surface growth and rupture in abdominal aortic aneurysm-application in a clinical paradigm. Ann Vasc Surg 2018;46:357–66. doi:10.1016/j.avsg.2017.08.007.
[46] van Disseldorp EMJ, Petterson NJ, Rutten MCM, van de Vosse FN, van Sambeek MRHM, Lopata RGP. Patient specific wall stress analysis and mechanical characterization of abdominal aortic aneurysms using 4d ultrasound. Eur J Vasc Endovasc Surg 2016;52:635–42. doi:10.1016/j.ejvs.2016.07.088.
[47] Martufi G, Satriano A, Moore RD, Vorp DA, Di Martino ES. Local quantification of wall thickness and intraluminal thrombus offer insight into the mechanical properties of the aneurysmal aorta. Ann Biomed Eng 2015;43:1759–71. doi:10.1007/s10439-014-1222-2.
[48] Hinnen J-W, Koning OHJ, Visser MJT, Van Bockel HJ. Effect of intraluminal thrombus on pressure transmission in the abdominal aortic aneurysm. J Vasc Surg 2005;42:1176–82. doi:10.1016/j.jvs.2005.08.027.
[49] Takashima K, Kitou T, Mori K, Ikeuchi K. Simulation and experimental observation of contact conditions between stents and artery models. Med Eng Phys 2007;29:326–35. doi:10.1016/j.medengphy.2006.04.003.
[50] Chu B, Mongrain R, Leask R, Bertrand OF. Stented coronary artery phantom for particle image velocimetry. CMBES Proc 2007;30(1) https://proceedings.cmbes.ca/index.php/proceedings/article/view/132.
[51] Yunker BE, Cordes D, Scherzinger AL, Dodd GD, Shandas R, Feng Y, et al. An investigation of industrial molding compounds for use in 3D ultrasound, MRI, and CT imaging phantoms. Med Phys 2013;40. doi:10.1118/1.4802083.
[52] Stepniak K, Ursani A, Paul N, Naguib H. Development of a phantom network for optimization of coronary artery disease imaging using computed tomography. Biomed Phys Eng Express 2019;5:045019. doi:10.1088/2057-1976/ab2696.
[53] Roehmbauer B. Mathematical and experimental development of two different stent models for PLV application. Department of Mechanical Engineering, Mcgill University; 2005.
[54] Klein A. Segmentation and motion estimation of stent grafts in abdominal aortic aneurysms. Enschede: University of Twente; 2011. doi:10.3990/1.9789036532662.
[55] Thubrikar MJ, F B, Labrosse M, Robicsek F, Al-Soudi J. Mechanical properties of abdominal aortic aneurysm wall. J Med Eng Technol 2001;25:133–42. doi:10.1080/03091900110057806.
[56] Wang DHJ, Makaroun M, Webster MW, Vorp DA. Mechanical properties and microstructure of intraluminal thrombus from abdominal aortic aneurysm. J Biomech Eng 2001;123:536–9. doi:10.1115/1.1411971.
[57] Kung EO, Les AS, Medina F, Wicker RB, McConnell MV, Taylor CA. In vitro validation of finite element model of aaa hemodynamics incorporating realistic outlet boundary conditions. J Biomech Eng 2011;133:041003. doi:10.1115/1.4003526.
[58] Russ C, Gessat M, Falk V, Szekely G. Rapid prototyping of silicone-based phantom models for stent simulation validation. Proceedings of the 15th International Conference on Medical Image Computing and Computer-Assisted Intervention, MICCAI. Nice: University of Zurich; 2012. p. 80–7. doi:10.5167/uzh-72940.
[59] Paramasivam S, Baltsavias G, Psatha E, Matis G, Valavanis A. Silicone models as basic training and research aid in endovascular neurointervention—a single-center experience and review of the literature. Neurosurg Rev 2014;37:331–7. doi:10.1007/s10143-014-0518-x.
[60] Wang Y, Joannic D, Juillion P, Monnet A, Delassus P, Lalande A, et al. Validation of the strain assessment of a phantom of abdominal aortic aneurysm: comparison of results obtained from magnetic resonance imaging and stereovision measurements. J Biomech Eng 2018;140:031001 -031001–9. doi:10.1115/1.4038743.
[61] Chayer B, van den Hoven Mvan den, Cardinal M-HR, Li H, Swillens A, Lopata R, et al. Atherosclerotic carotid bifurcation phantoms with stenotic soft inclusions for ultrasound flow and vessel wall elastography imaging. Phys Med Biol 2019;64:095025. doi:10.1088/1361-6560/ab1145.
[62] Mix DS, Stoner MC, Day SW, Richards MS. Manufacturing abdominal aorta hydrogel tissue-mimicking phantoms for ultrasound elastography validation. JoVE J Vis Exp 2018:e57984. doi:10.3791/57984.
[63] Polanczyk A, Podgorski M, Polanczyk M, Piechota-Polanczyk A, Neumayer C, Stefanczyk L. A novel patient-specific human cardiovascular system phantom (hcsp) for reconstructions of pulsatile blood hemodynamic inside abdominal aortic aneurysm. IEEE Access 2018;6:61896–903. doi:10.1109/ACCESS.2018.2876377.
[64] Chen T, Lancaster M, Lin DSY, Doyle MG, Forbes TL, Amon CH. Measurement of frictional properties of aortic stent grafts and their delivery systems. J Med Devices 2019;13. doi:10.1115/1.4043292.
[65] Kontopodis N, Metaxa E, Pagonidis K, Ioannou C, Papaharilaou Y. Deformation and distensibility distribution along the abdominal aorta in the presence of aneurysmal dilatation. J Cardiovasc Surg 2017;58:72–9. doi:10.23736/S0021-9509.16.07737-5.
[66] Zha Y, Peng G, Li L, Yang C, Lu X, Peng Z. Quantitative aortic distensibility measurement using ct in patients with abdominal aortic aneurysm: reproducibility and clinical relevance. BioMed Res Int 2017;2017. doi:10.1155/2017/5436927.
[67] Roy D, Holzapfel GA, Kauffmann C, Soulez G. Finite element analysis of abdominal aortic aneurysms: geometrical and structural reconstruction with application of an anisotropic material model. IMA J Appl Math 2014;79:1011–26. doi:10.1093/imamat/hxu037.
[68] Gindre J, Bel-Brunon A, Rochette M, Lucas A, Kaladji A, Haigron P, et al. Patient-specific finite-element simulation of the insertion of guidewire during an evar procedure: guidewire position prediction validation on 28 cases. IEEE Trans Biomed Eng 2017;64:1057–66. doi:10.1109/TBME.2016.2587362.
[69] Liu Y, Dang C, Garcia M, Gregersen H, Kassab GS. Surrounding tissues affect the passive mechanics of the vessel wall: theory and experiment. Am J Physiol Heart Circ Physiol 2007;293:H3290–300. doi:10.1152/ajpheart.00666.2007.
[70] Mohammadi H, Lessard S, Therasse E, Mongrain R, Soulez G. A numerical preoperative planning model to predict arterial deformations in endovascular aortic aneurysm repair. Ann Biomed Eng 2018;46:2148–61. doi:10.1007/s10439-018-2093-8.
[71] Gong JP. Friction and lubrication of hydrogels—its richness and complexity. Soft Matter 2006;2:544–52. doi:10.1039/B603209P.